Hindawi
Adsorption Science & Technology
Volume 2021, Article ID 6619389, 14 pages
https://doi.org/10.1155/2021/6619389

Research Article

Application of Innovative Analytical Modeling for the Physicochemical Analysis of Adsorption Isotherms of Silver Nitrate on Helicenes: Phenomenological Study of the Complexation Process

Hanen Souissi and Mohamed Ben Yahia

Laboratory of Quantum and Statistical Physics LR18ES18, Faculty of Sciences of Monastir, University of Monastir, Tunisia

Correspondence should be addressed to Mohamed Ben Yahia; ben_yahia_med@hotmail.fra

Received 15 July 2020; Accepted 16 December 2020; Published 15 January 2021

Academic Editor: Adrián Bonilla Petriciolet

The interaction between the silver ion and the cyclic aromatic molecules, namely, the helicenes, is the subject of this paper. In fact, a silver complexation system based on quartz crystal microbalance (QCM) sensor with a functional film of helicenes has been designed and developed at four temperatures. The developed system, in which the sensor response reflects the adsorption of the hexahelicene and the heptahelicene, was able to control the complexed mass of silver for each concentration. Experimental outcomes indicated that the quartz crystal coated with heptahelicene is the adequate material for silver adsorption. Then, a theoretical study has been performed through two statistical physics models (SMPG and SMRG) in order to analyze the experimental adsorption isotherms of the two helicenes at the ionic scale. The SMRG model was developed using the real gas law and was satisfactorily applied for the microscopic investigation of the hexahelicene isotherms indicating that the lateral interactions between the adsorbates are responsible of the decrease of the adsorbed quantity at saturation. The interpretation of the two models' parameters indicated that the adsorption of the two helicenes is an endothermic phenomenon. Interestingly, the heptahelicene is recommended for silver complexation because it shows the highest adsorption energies involving chemical bonds during the complexation process. The SMPG model and the SMRG model also allow prediction of three thermodynamic functions (configurational entropy, Gibbs free enthalpy, and internal energy) which govern the adsorption mechanism of silver on the two helicenes.

1. Introduction

The hexahelicene and the heptahelicene are interesting members of the carbohelicene family which provide a central cavity suitable for complexing cationic ions [1, 2]. These molecules are characterized by their helical geometry and their extraordinary electronic properties ([3–5], and they are involved in numerous fields of research including molecular recognition [6, 7], supramolecular chemistry [8], and catalysis of transition metal [9]. The profile of these molecules shows the two terminal rings of benzene overlapping like "jaws of a crocodile" which permits their use for the advancement of the metallic sandwich systems in organometallic chemistry [10, 11]. The complexation of helicenes by metals suggests the construction of future devices in optoelectronics as the chiral waveguides. We can also think of the design of new materials for the modulation of information in the telecommunications field ([12]). So, it is intriguing to check if these small molecules have the adequate adaptability to complex the cationic metals [13, 14].

In this way, it has been recently shown that the hexahelicene and the heptahelicene can complex the alkali metals (K^+, Li^+, …) [15, 16]. Other examinations suggested that the hexahelicene can complex the metallic silver ion (Ag^+) (Figure 1(a)) [17]. However, the binding of the silver particle in the focal cavity of hexahelicene has been exhibited, given

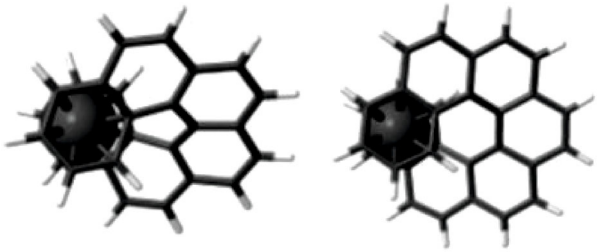

(a) (b)

Figure 1: Illustration of the (a) silver-[6]helicene complex and the (b) silver-[7]helicene complex.

that the counter ion is quickly coordinating. In this coupling mode, the hexahelicene is working as a chiral molecular tweezer of silver but the resulting bond is not strong and the formed complex is not stable [18, 19].

On the other hand, until now, no deep investigation has been performed to use the heptahelicene as a complexing compound of silver despite the importance of the silver-heptahelicene complex (Figure 1(b)) in several interesting fields; for example, it can be used for the construction of solid-state devices (e.g., electric conductors [20]). This is surprising since the previously studied complexes indicated that the complexes of heptahelicene were more stable than the corresponding complexes of hexahelicene [21]. Therefore, in this work, a quartz crystal microbalance (QCM) ([15, 22] is used to control the interaction between the univalent silver ion (Ag^+) and the two helicenes (the hexahelicene and the heptahelicene).

The QCM strategy includes the preparation of thin film of composite doped on quartz crystal which permits outstanding control over the adsorbed film thickness. Other techniques have been adopted to cover the electrode surface with similar composites, e.g., direct adsorption, incorporation inside PVC or other inert polymer matrices, and polymerization-deposition of the species of interest on the electrode surface [23]. But the quartz crystal microbalance was more effective than the other methods [24]. The QCM strategy involves the spin coating of helicene volume on the quartz electrode to cover the overlapping electrode portion. The goal is to obtain appropriate films which should be homogeneous over the whole surface of the quartz crystal [25, 26]. Indeed, the first part of this work is aimed at controlling the adsorbed mass of silver on helicene layers at different temperatures using the QCM apparatus [26, 27]. The second part is devoted to the modeling of these isotherms using the adsorption models developed through statistical physics treatment [28]. The interpretation of the physicochemical parameters involved in the statistical physics models plays a crucial role in the selection of the best complexing adsorbent of silver regarding its stability and reactivity.

In summary, three goals are suggested in this research work: (1) confirming that the helicene molecules (the hexahelicene and the heptahelicene) can function as sensors of the silver ion, (2) choosing the appropriate adsorbent for silver complexation by analyzing the experimental results: the selection of the best adsorbent depends on the comparison of the adsorption capacities of the hexahelicene and the heptahelicene, and (3) interpreting the complexation mechanism at the ionic level through the parameters involved in the statistical physics models and verifying the choice of the best adsorbent through an energetic study.

2. Materials and Methods

For many years, the QCM has been considered as a gas phase mass detector. In 1959, Sauerbrey [29] introduced a relation giving the variation of the resonant frequency of the quartz according to the deposited mass. Then, Nomura and Okuhara [30] demonstrated that the piezoelectric quartz crystal can oscillate in a liquid medium. They thought about its application at the solid-liquid interface. The progress of the QCM application motivated us to use this experimental approach for the measurement of the adsorption isotherms of helicenes.

2.1. Experimental Setup Description. Figure 2 represents the experimental setup of the QCM strategy.

The piezoelectric quartz crystal is the main constituent of the QCM setup. Natural or synthetic quartz crystal is cut in a specific orientation around the OY axis giving rise mainly to two types of thin disc: AT and BT. The AT cut is used in this work because it is the best known cut since 1934. It constitutes most of all the crystals (around 90%) [31]. This cut is used for a frequency ranging from 0.5 to 300 MHz. They are sensitive to the mechanical constraints caused by the external forces or by the temperature gradients. The quartz crystals used in these experiments are covered on both sides with gold of thickness varying from 100 to 1000 nm. The thickness of the crystal is about 331 μm. It should be also noted that the crystals used are polished and have a diameter of 2.54 cm.

The preparation of the adsorption cell requires the cleaning of the gold electrode of the quartz crystal and the deposition of the substrate on the quartz surface. First of all, the layer of resin, which is applied to protect the crystal surface, was removed using a well-defined cleaning protocol [32]. The disc was rinsed with acetone and deionizer water followed with drying. Then, the gold electrode was cleaned with a Piranha solution at room temperature for 1 to 5 minutes. After this cleaning treatment, the crystals were thoroughly rinsed with deionizer water and ethanol and dried by applying high purity nitrogen to remove any remaining water. The resonant frequency of the blank crystal was recorded. Then, the functionalization of the active surface of the crystal was carried out by spin coating of the adsorbent (the hexahelicene or the heptahelicene) solution. For film deposition, a volume of 40 μL of the adsorbent was spin coated at 3000 rpm for 1 minute on the largest gold electrode. The coated crystals were then dried at 100°C for at least 2 h. The goal was to obtain a uniform deposited film over the entire crystal surface. Then, the resonant frequency of the quartz crystal coated with the helicene film was measured. Thus, we have ensured that the deposited film of helicenes produced a variation of the resonant frequency of the quartz crystal which makes sure the presence of functionalized film on chip surface. Using the Sauerbrey equation (Equation (2)),

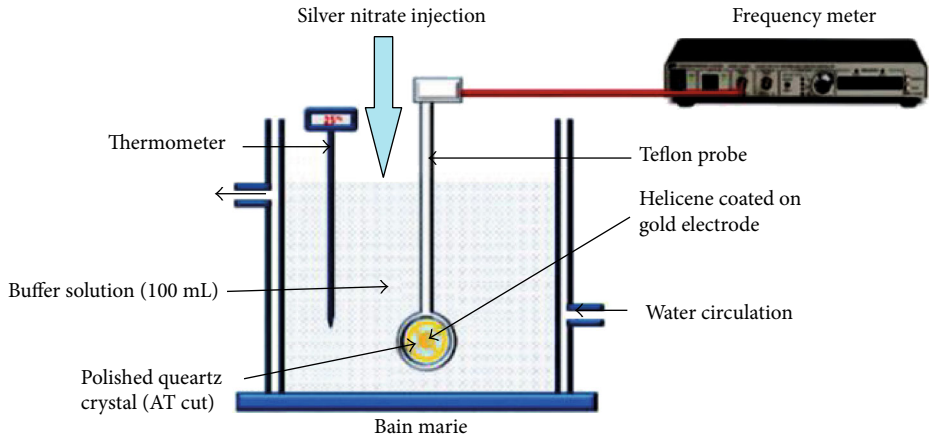

Figure 2: Experimental setup of the quartz crystal microbalance (QCM) devoted for the measurement of the experimental adsorption isotherms of silver nitrate on heptahelicene and hexahelicene.

the mass of the deposited helicenes on adsorption cell was calculated by the intermediate of the difference between the frequencies of the blank crystal and the coated crystal. The mass of the helicene film per unit of surface is about 209.9 μg/cm^2. It should be noted that the frequency of the coated crystal with hexahelicene is almost equal to the frequency of the coated crystal with heptahelicene since the quartz crystals were functionalized with the same volume of the two helicenes under the same experimental conditions. This confirms that the two different helicenes formed the same type of film. It should be also noticed that the determination of the adsorbed mass of silver onto the adsorption cell did not include the effect of the helicene film. This can be demonstrated by Equation (4) which shows clearly that the variation of the resonant frequency of the quartz crystal Δf is only due to the mass variation Δm of silver and does not include the effect of the deposited mass of helicenes since the frequency F_0, which characterizes the deposited helicene film and the effect of the hydrostatic pressure in the reactor, is eliminated from the frequency variation Δf.

After drying, the adsorption cell (crystal coated with helicenes) was inserted into the Teflon probe. We noticed that a wrong orientation of the quartz crystal in the probe leads to a malfunction of the QCM. This was resolved by placing the crystal in a probe alignment mark. Then, we operated by a rotation of the crystal with an angle of 90° in the positive direction. A ring was placed in front of the crystal to protect the electrode from the penetration of the liquid in the Teflon probe. The connection of the probe with the monitor was assured by means of a coaxial cable. During the experiments, the frequency variation was computed by a Maxtek PM700 frequency meter. Note that a thermometer was used to control the temperature in the reactor during the isotherm measurement. Thus, the thermal equilibrium was ensured by water circulation around the adsorption cell through a bain-marie which was maintained at a constant temperature.

2.2. Measurement Protocol

2.2.1. Sauerbrey's Equation. The quartz crystal is formed by a pair of electrodes that connects the two sides which ensures the connection to the oscillator circuit and the contact with the experimental environment. The piezoelectric crystal, which is covered with gold layer on the two sides, is brought into resonance by means of an alternating electric current. The alternating voltage induces the oscillation of the crystal at the resonant frequency [33]. The disturbance at the crystal surface affects immediately the oscillation frequency; therefore, the experiments should be carried out in a tightly closed system for best results. The resonant frequency is determined with accuracy usually less than 1 Hz. The quantity of adsorbed material on the crystal surface is determined with a detection limit of 5 ng/cm^2 in liquid medium using a quartz crystal of 5 MHz [33]. The slight mass variation of one of the electrodes induces a slight decrease in the quartz resonance frequency. This effect is modeled by the Sauerbrey equation [29] which links the mass variation on the electrodes Δm to the resonant frequency variation Δf. Thus, Sauerbrey hypothesized that for small mass change, the added mass could be treated as an additional mass of the quartz. The linear relationship between the frequency change (Δf) and the mass variation (Δm) is expressed as follows [29, 34]:

$$\Delta f = -\left(\frac{2 \cdot f_0^2}{A \cdot \rho \cdot \upsilon}\right) \cdot \Delta m, \quad (1)$$

where A is the area of the sensitive surface of quartz (cm^2), ρ is the crystal density (g/cm^3), υ is the propagation speed of the acoustic wave (3336×10^5cm/s), f_0 is the resonant frequency of the crystal before deposition (Hz), Δf is the resonant frequency variation (Hz), and Δm is the deposited mass on the quartz (μg/cm^2).

This equation is called the Sauerbrey equation which can be also written as [29, 35]

$$\Delta m = -\frac{\Delta f}{C}. \quad (2)$$

This equation introduces the Sauerbrey constant C (Hz·cm^2/μg) which is the specific characteristic of the crystal and describes the linear sensitivity factor. Note also that the

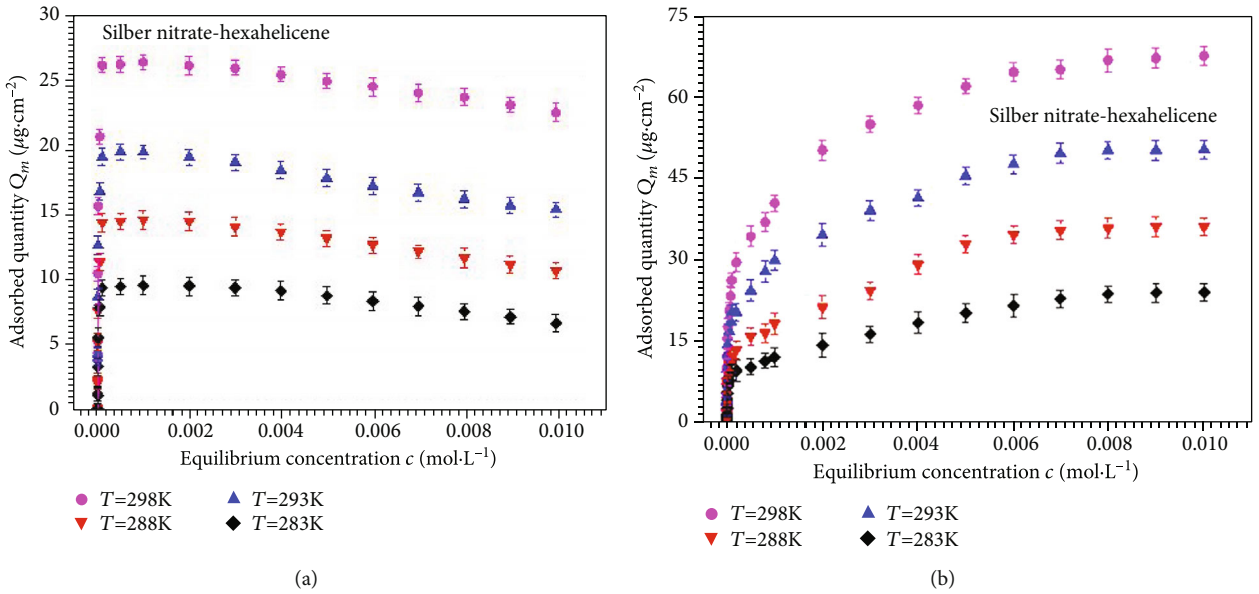

Figure 3: Equilibrium adsorption isotherms of silver nitrate onto hexahelicene and heptahelicene given at four temperatures (283-298 K).

resonant frequency of a quartz crystal (5 MHz) can be measured with an accuracy of 0.01 Hz in vacuum and 0.1 Hz in liquids. Accordingly, very small masses of the nanogram scale can be measured with the QCM.

2.2.2. Isotherm Measurement. In the reactor filled with the buffer solution ($V_s = 100$ mL), the adsorption cell was immersed until the stabilization of the crystal frequency. Once the crystal was immerged in water, a frequency change was observed due to the hydrostatic pressure. This resonant frequency of the coated crystal was noted F_0 (Hz) and was used as reference in our measurement. Then, volumes of adsorbate ($AgNO_3$) were injected in order to increase the silver concentration in the reactor.

Adding a volume V_{ad} (μL) to the initial volume V_s (100 mL) allowed obtaining concentrations of solution ranging from 10^{-7} mol·L^{-1} to 0.01 mol·L^{-1}. If we note by $c_0 = 10^{-4}$ mol · L^{-1} the concentration of the buffer solution of silver nitrate already prepared and we want to obtain a final concentration in the reactor $c_f = 10^{-7}$ mol · L^{-1}, the added volume can be calculated based on the law of conservation of matter as follows:

$$V_{ad} = \frac{c_f \times V_s}{c_0}. \quad (3)$$

The added volumes for each concentration were calculated according to the last equation, and the additions were made using a micropipette. For example, to obtain the concentration 10^{-7} mol·L^{-1}, 100 μL of silver nitrate solution (10^{-4} mol·L^{-1}) was injected into the reactor followed by magnetic stirring for 5 min to homogenize the solution. This step was repeated according to the number of performed injections which led to obtain solutions of increasing concentration. After each addition, the quartz microbalance displayed the resonance frequency associated with the new concentration. The frequency variation after every injection was determined by the following equation:

$$\Delta f = F_i - F_0, \quad (4)$$

where F_i (Hz) is the measured frequency after injection i and F_0 (Hz) is the frequency of the coated crystal in the reactor.

In this manner, we directly apply the Sauerbrey relation (Equation (2)) to deduce the adsorbed mass (Δm). It should be noted that the mass variation Δm is also noted Q_m (μg/cm^2) which represents the adsorbed quantity. We can finally deduce the complexed quantity per unit of surface area for each concentration.

The equilibrium adsorption isotherms of silver nitrate onto the two supports of the hexahelicene and the heptahelicene are represented at 283-298 K in Figure 3.

2.3. Discussion of Experimental Results. Based on the experimental isotherm profiles, we note the following results.

Firstly, the experimental adsorption isotherms indicated that the silver particles are captured by the hexahelicene and the heptahelicene at various temperatures. Therefore, it is demonstrated that the two helicenes can function as "sandwich" systems of the silver ions.

Secondly, one can see that the behaviors of the isotherm curves are different for the two helicenes, despite the fact that all the experimental data were measured under the same conditions. One can conclude that the isotherm profile depends on the adsorbent type which constitutes the dominant factor of the complexation phenomenon. Moreover, by looking at the adsorbed amounts of the two helicenes, we hold that the heptahelicene presents the highest adsorption capacities, and consequently, it is the best adsorbent for silver complexation.

Finally, it is noticed that the experimental isotherms present one saturation level indicating that only one layer of the cationic ions Ag^+ is adsorbed onto the two solid supports of the hexahelicene and the heptahelicene. The nitrate ions are

not associated with the adsorption system of silver nitrate and do not participate at the layer formation in keeping with the previous studies of the adsorption of potassium chloride onto comparative adsorbent [28]. However, the distinction between the isotherms of the two helicenes altogether appeared at saturation. At high adsorbate concentration, we can see a stable saturation state for the heptahelicene which means that all the receptor sites are occupied and that the $AgNO_3$-heptahelicene interaction is strong so cutting this link is almost impossible. For hexahelicene adsorption, one saturation level followed with a drop is observed at the four temperatures which suggests the presence of an opposite phenomenon (desorption process) after the saturation state. This can be explained by the fact that the $AgNO_3$-hexahelicene bond is weak so the silver ions can escape from the crocodile jaws (the hexahelicene cavity) at any time which leads to the decrease of the adsorbed quantity at high concentration. According to these explanations, one can conclude that the heptahelicene is the suitable adsorbent for silver complexation.

In the next section, statistical physics treatment is proposed for modeling analysis of the adsorption isotherms [36, 37]. The goal is to elaborate a theoretical description of these experimental results at the ionic scale.

3. Statistical Physics Modeling

In the experimental part, it is noted that the microscopic investigation of the complexation reactions needs the application of two statistical physics models: single-layer model with stable saturation level for the heptahelicene adsorption and single-layer model with unstable saturation state for the hexahelicene adsorption. The modeling work is then arranged as follows. Firstly, we review the methodology of statistical physics formalism beginning from the grand canonical ensemble to the final adsorbed quantity expression. Secondly, the statistical physics model which will be applied for the interpretation of the adsorption isotherms is selected through numerical simulation. Finally, based on fitting the experimental isotherms with the adsorption models, the complexation process is evaluated and interpreted by the intermediate of the parameters of the selected model.

3.1. Advanced Adsorption Models. Overall, from the statistical physics models, the physical parameter values deduced from numerical simulation are used to investigate the adsorption process at the ionic scale if the adsorbate and the adsorbent properties are well known. The first progress of this advanced treatment is observed against the oldest empirical equation elaborated by Langmuir et al. [38]. Langmuir assumed that an adsorbent site can integrate only one particle; however, our statistical physics models proposed that one receptor site can suit n particles where n is a variable number. In addition, our statistical physics models suggested the presence of various adsorption energies that are related to various receptor sites, contrary to the empirical models (Langmuir and Freundlich) [38, 39] which accept the presence of one adsorption energy level for all adsorbent sites.

In the present examination, the helicene adsorption isotherms can be interpreted by a single-layer model that describes two types of sites. The choice of this model among the others is not arbitrary but based on physical reasons. In reality, the analytical development of this model requires to take account of the two spatial conformations (M and P) of the two members of the helicene family (the hexahelicene and the heptahelicene) [40]. In this manner, the adsorbent sites can be divided into two types of receptors whose densities are H_{m1} and H_{m2}. So, it is suggested that the adsorption of silver onto H_{m1} occurs with an energy level $(-E_1)$ while the adsorption onto H_{m2} takes place via the energy $(-E_2)$.

According to the statistical physics methodology, the first step of the analytical development is the partition function of the grand canonical ensemble of Gibbs (z_{gc}) which has the following expression [15]:

$$\begin{aligned} z_{1gc} &= 1 + e^{\beta(E_1+\mu_1)}, \\ z_{2gc} &= 1 + e^{\beta(E_2+\mu_2)}, \end{aligned} \tag{5}$$

where z_{1gc} is the partition function of one receptor site of the first type of sites H_{m1}, z_{2gc} is the partition function of one receptor site of the second type of sites H_{m2}, and $\beta = 1/k_B T$ is the Boltzmann factor with T being the temperature (K) and k_B being the Boltzmann coefficient ($1.3806488 \times 10^{-23}$ JK^{-1}). μ_1 (kJ/mol) and μ_2 (kJ/mol) are the chemical potentials of the adsorbed particle on the two types of sites.

The second step of the models' development involves the determination of the average occupancy numbers (N_{01} and N_{02}) of independent helicene sites using the following equations [37, 41]:

$$\begin{aligned} N_{01} &= \frac{H_{m1}}{1 + e^{-\beta(E_1+\mu_1)}}, \\ N_{02} &= \frac{H_{m2}}{1 + e^{-\beta(E_2+\mu_2)}}. \end{aligned} \tag{6}$$

Overall, the isotherms' curves of heptahelicene show a stable saturation level without dropping at high concentration. In this case, we apply the chemical potential coupled to the ideal gas approach. In the presence of this mean potential, we can consider that one individual particle has no interaction with the rest of the system like an ideal fermion gas of electrons. It can be written as follows [36, 41]:

$$\mu_p = \frac{1}{\beta} \ln\left(\frac{N}{z_{Tr}}\right), \tag{7}$$

with N being the number of adsorbates and z_{Tr} being the translation partition function which can be written as [16]

$$z_{Tr} = V\left(\frac{2\pi m k_B T}{h^2}\right)^{3/2}, \tag{8}$$

where m is the mass of an adsorbed particle, V is the volume of an individual adsorbate, and h is the constant of Planck

($6.62606957 \times 10^{-34}$ J · s). Note that the investigated silver ion in this paper is monoatomic. So there are no vibrational and no rotational degrees of freedoms for a monoatomic ion. Electronic and obviously nuclear degrees of freedom are frozen. The only degree of freedom which can be excited is the translational one [15, 16].

On the other hand, the hexahelicene isotherms show a downward trend at the four temperatures (unstable saturation state). For each temperature, despite the increase of the adsorbate concentration, the adsorbed quantity decreases. According to previous works, the reversible phenomenon at the saturation state is basically due to the lateral interactions between the adsorbates which are described by the cohesion pressure a and the covolume b [15, 37].

At high silver nitrate concentration, the adsorbate-adsorbate interaction (lateral interaction) is higher than the adsorbate-adsorbent interaction which means that the adsorbate particles are more attractive with the solution than with the helicene surface leading to a decline of the adsorbed quantity. Indeed, the problem of lateral interaction between adsorbate molecules/ions either at the free state or at the adsorbed state is very complex to be easily quantified. However, to take account of this interaction, an indirect method is applied to quantify this effect by using the adequate statistical ensemble which is the grand canonical ensemble, favorable ensemble to calculate such interactions. In this manner, in order to describe the high concentration adsorption equilibrium, the statistical physics modeling should be performed by applying the chemical potential corresponding to the real gas μ_r (kJ/mol) in which the Van der Waals variables are introduced [15, 16].

$$\mu_r = \mu_p + \frac{1}{\beta} \ln \frac{1}{1-bc} + \frac{1}{\beta}\frac{bc}{1-bc} - 2ac, \tag{9}$$

where μ_p (kJ/mol) is expressed by Equation (7), c is the adsorbate concentration (mol·L^{-1}), a is the cohesion pressure (J·mL·mol^{-1}), and b is the covolume (mL·mol^{-1}).

Finally, the analytical expression of the adsorbed quantity Q_m (μg/cm^2) can be calculated as follows [41]:

$$Q_m = n_1 \cdot N_{01} + n_2 \cdot N_{02}, \tag{10}$$

where n_1 is the number of silver per site M and n_2 is the number of silver per site P.

For heptahelicene adsorption, the single-layer model (ideal gas approach) is expressed as

$$Q_{SMPG} = \frac{Q_{S1}}{1 + (c_1/c)^{n_1}} + \frac{Q_{S2}}{1 + (c_2/c)^{n_2}}, \tag{11}$$

where $Q_{S1} = n_1 * H_{m1}$ (μg/cm^2) and $Q_{S2} = n_2 * H_{m2}$ (μg/cm^2) are the adsorbed amounts at saturation of the two types of sites M and P. c_1 (mol·L^{-1}) and c_2 (mol·L^{-1}) are energetic parameters given by

$$\begin{aligned} c_1 &= c_s e^{-\Delta E_1/RT}, \\ c_2 &= c_s e^{-\Delta E_2/RT}, \end{aligned} \tag{12}$$

where c_s is the solubility of adsorbate in aqueous solution (mol·L^{-1}), $-\Delta E_1$ is the molar adsorption energy of the first type of sites (kJ/mol), $-\Delta E_2$ is the molar adsorption energy of the second type of sites (kJ/mol), R is the ideal gas constant (8.3144621 J·mol^{-1}·K^{-1}), and T is the adsorption temperature (K).

For hexahelicene adsorption, the single-layer model (real gas approach) is given as follows:

$$\begin{aligned} Q_{SMRG} = {} & \frac{Q_{S1}}{1 + \left(w_1((1-bc)/c)e^{2\beta ac}e^{-bc/(1-bc)}\right)^{n_1}} \\ & + \frac{Q_{S2}}{1 + \left(w_2((1-bc)/c)e^{2\beta ac}e^{-bc/(1-bc)}\right)^{n_2}}. \end{aligned} \tag{13}$$

This advanced model presents six physicochemical parameters: two adsorbed quantities at saturation Q_{S1} (μg/cm^2) and Q_{S2} (μg/cm^2), two parameters describing the lateral interactions a (J·mL·mol^{-1}) and b (mL·mol^{-1}), and two parameters involving energetic aspect w_1 (mol·L^{-1}) and w_2 (mol·L^{-1}) which are expressed as

$$\begin{aligned} w_1 &= c_s e^{-\Delta E_1/RT}, \\ w_2 &= c_s e^{-\Delta E_2/RT}. \end{aligned} \tag{14}$$

All variables are previously declared.

3.2. Numerical Adjustment. Numerical fitting program is used to evaluate the coherence between the adsorption isotherms and the two advanced models. The mathematical fitting method is based on the Levenberg-Marquardt iterating algorithm using a multivariable nonlinear regression program. The best fitting result is established once the residuals between the experimental and the theoretical values by the model are minimized according to a determined level of confidence [42]. In our case, the level of confidence was set at 95%. Remember that three error coefficients are deduced from the numerical simulation of the experimental isotherms with the developed models [43].

The first fitting criterion is the well-known multiple correlation coefficients squared, R^2, also known as the coefficient of determination which is a standardized measure of the goodness of fit [42, 43]. A very common procedure for choosing among alternative models is to select the one that fits the best, that is, the one that has the highest coefficient of determination R^2. The ideal fitting is obtained when the value of R^2 is close to the unit.

The second coefficient is the residual root mean square error (RMSE) also called the estimated standard error of the regression which is a nonstandardized measure of the goodness of fit [43, 44]. The value of root mean square error (RMSE) shows that the fitting ability of the modeling related to the number of data points is minimal for the best model. If the model is correct and the parameter estimates unbiased,

Table 1: Values of the Correlation coefficient R^2, the Residual root mean square error coefficient RMSE and the Akaike information criterion AIC deduced from fitting the experimental adsorption isotherms of silver nitrate on helicenes with the two single-layer adsorption models (SMPG and SMRG).

Adsorption system/fitting model	Temperature(K)	Correlation coefficient R^2	Residual root mean square error RMSE	Akaike information criterion AIC
$AgNO_3$-[7]helicene/ SMPG	**283K**	0.99	0.031	7.2
	288K	0.98	0.03	6.3
	293K	0.99	0.044	5.4
	298K	0.98	0.036	3.3
$AgNO_3$-[7]helicene/ SMRG	**283K**	0.95	1.9	13.2
	288K	0.94	2.2	13.9
	293K	0.95	1.91	12.2
	298K	0.91	2.4	12.5
$AgNO_3$-[6]helicene/ SMPG	**283K**	0.88	3.1	15.8
	288K	0.85	3.5	15.9
	293K	0.85	3.3	14.9
	298K	0.86	2.9	14.2
$AgNO_3$-[6]helicene/ SMRG	**283K**	0.99	0.61	9.9
	288K	0.99	0.94	9.2
	293K	0.97	0.83	8.4
	298K	0.99	0.81	9.1

then approximately 95% of the estimated values should fall within ±1 RMSE of their true values.

The third error coefficient is the Akaike Information Criterion (AIC) which is a fitting criterion of comparison of the adjustment with the two models: the model with the lowest AIC values is the most appropriate for the theoretical description of the experimental isotherms [45].

The two single-layer models (SMPG and SMRG) were applied on the adsorption isotherms, and the values of the error coefficients of the adjustment (R^2, RMSE, and AIC) are listed in Table 1.

According to Table 1, a good correlation of the SMPG model is obtained with the experimental data of heptahelicene since we found that $R^2 \approx 1$, RMSE < 1, and AIC are the lowest values. However, in light of the selection criteria, the SMRG model is chosen for the theoretical description of the hexahelicene isotherms (R^2 ranging from 0.97 to 0.99 and RMSE and AIC are the smallest quantities) which promotes to confirm that the decline of the adsorbed amount after the saturation is fundamentally due to the lateral interaction impacts. This numerical outcome is in correlation with the experimental result: the heptahelicene is confirmed to be the best complexing adsorbent of silver ions in terms of stability.

The usefulness of the advanced models is that their parameters are in good relation with the complexation processes. Hence, a deeper description of the two complexation systems is elaborated in the next stage using the numerical values of the models' parameters.

3.3. Physicochemical Interpretation. Figure 4 illustrates the evolutions of the fitting values of the physicochemical parameters as a function of temperature.

3.3.1. Steric Parameters. In Figure 4(a), the fitting values of the adsorbed amounts at saturation are plotted as a function of temperature for the two complexation systems Ag-[6]helicene and Ag-[7]helicene.

From Figure 4(a), we note that Q_{S1} ([7]helicene) > Q_{S1} ([6]helicene) and Q_{S2}([7]helicene) > Q_{S2} ([6]helicene). Therefore, it is concluded that the heptahelicene is more suitable for silver complexation in terms of quantity. It is also noticed that the adsorbed amounts at saturation Q_{S1} and Q_{S2} increase by expanding the temperature for the two complexing helicenes. The increment of these two parameters can result from the thermal agitation impact which activates more helicene sites to contribute to the complexation mechanisms. We conclude that the temperature enhances the complexation of silver ions and that the silver adsorption is an endothermic phenomenon regardless of the complexing adsorbent [45].

3.3.2. Van der Waals Parameter Behaviors. The Van der Waals parameters *a* and *b* are introduced in the SMRG model in order to ameliorate the physical description of the complexation process of the hexahelicene at high concentration [22, 46]. The behaviors of these parameters via the temperature are illustrated in Figure 4(b).

It can be noted from Figure 4(b) that the parameter *a* decreases with rising of the temperature which means that this parameter acts powerfully at low temperatures, i.e., the interaction between the adsorbates is low at high temperature. On the contrary, it is noted that the rise of the temperature causes a growth of the covolume *b* which means that the repulsion between the adsorbate ions becomes strong at high temperature. Therefore, it is concluded that the silver ions are quickly captured by the adsorbing surface of hexahelicene at high temperature which explains

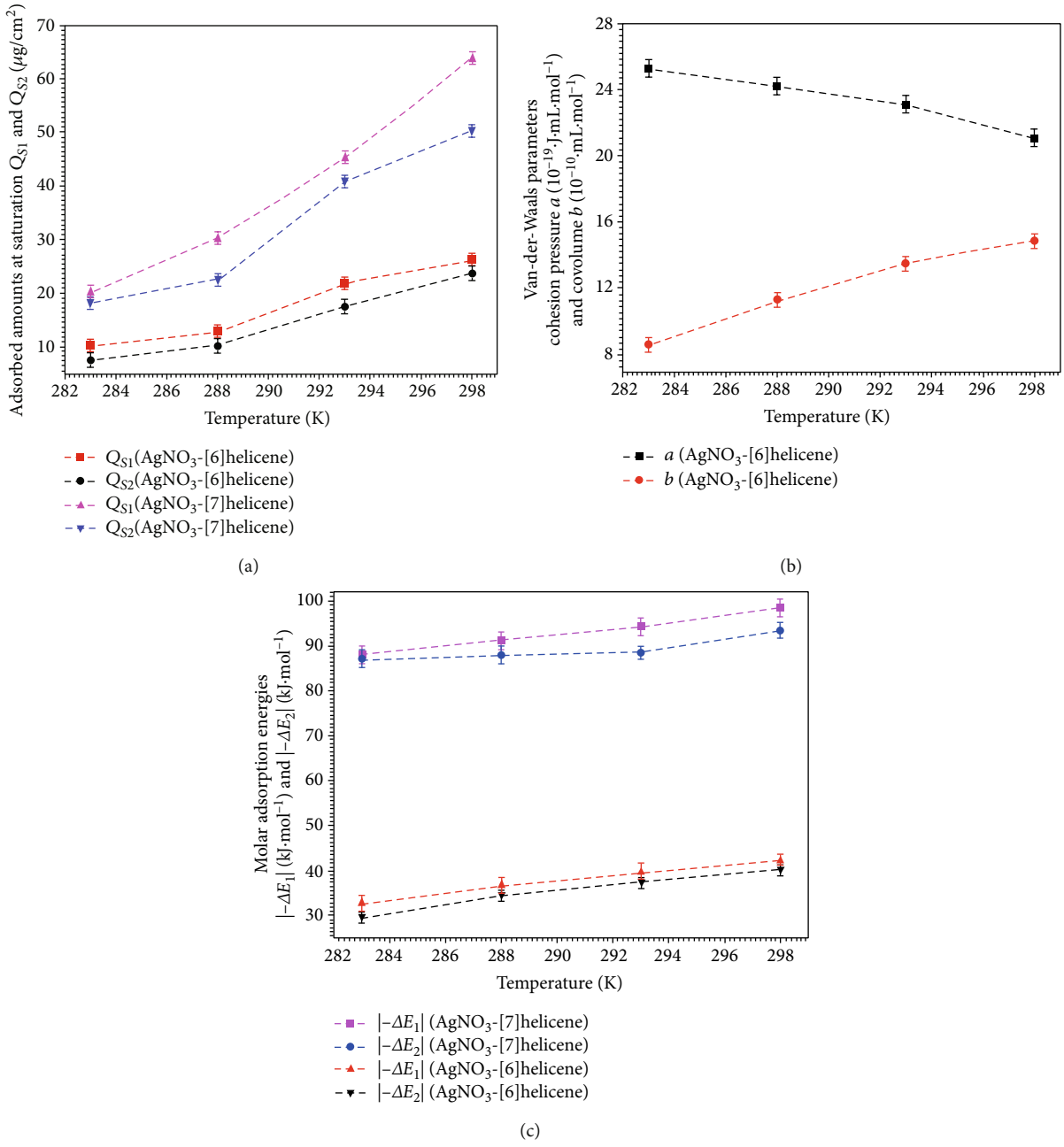

FIGURE 4: Evolutions of the (a) steric parameters Q_{S1} (μg·cm^{-2}) and Q_{S2} (μg·cm^{-2}), (b) the Van der Waals variables a (10^{-19}·J·mL·mol^{-1}) and b (10^{-10}·mL·mol^{-1}), and (c) the molar adsorption energies ($-\Delta E_1$ (kJ/mol) and $-\Delta E_2$) (kJ/mol) as a function of temperature.

the high performance of silver adsorption at high temperature and demonstrates the endothermic nature of the complexation process [46]. This suggests that the complexation of the hexahelicene by the silver ions can be carried out without disruptive influences if we increase further the adsorption temperature.

3.3.3. Energetic Calculation. The adsorption processes are necessarily evaluated on the basis of the models' parameters. In particular, the selection of the best adsorption system is dependent on the nature of the interaction between the silver and the two helicenes [15, 22]. Indeed, the description and identification of the interaction type is carried out through adsorption energy calculation. The adjusted values of the energetic parameters c_1 and c_2 of the SMPG model (heptahelicene adsorption) and w_1 and w_2 of the SMRG model (hexahelicene adsorption) deduced from the fitting of the experimental isotherms with the two models are used to calculate the molar adsorption energies ($-\Delta E_1$ and $-\Delta E_2$) of the two complexation systems.

For silver-heptahelicene,

$$-\Delta E_{1,2} = RT * \ln\left(\frac{c_{1,2}}{c_s(\mathrm{AgNO_3})}\right). \quad (15)$$

Table 2: Modulus values of the molar adsorption energies $|-\Delta E_1|$ (kJ/mol) and $|-\Delta E_2|$ (kJ/mol) describing the complexation of the two helicenes by the silver ions given at 283K, 288K, 293K and 298K.

Adsorption system	Temperature (K)	$\|-\Delta E_1\|$(kJ/mol)	$\|-\Delta E_2\|$(kJ/mol)
$AgNO_3$-[7]helicene	**283K**	88.1	86.9
	288K	91.6	88.1
	293K	94.4	88.6
	298K	98.5	93.5
$AgNO_3$-[6]helicene	**283K**	32.5	29.5
	288K	36.6	34.4
	293K	39.5	37.5
	298K	42.2	40.3

For silver-hexahelicene,

$$-\Delta E_{1,2} = RT * \ln\left(\frac{w_{1,2}}{c_s(AgNO_3)}\right), \tag{16}$$

where $c_s(AgNO_3)$ is the silver nitrate solubility (mol·L^{-1}).

The values of the molar adsorption energies are given in Table 2.

According to Table 2, it can be noted that $|(-\Delta E_1)|$ ([7]helicene) > $|(-\Delta E_1)|$ ([6]helicene) and $|(-\Delta E_2)|$ ([7]helicene) > $|(-\Delta E_2)|$ ([6]helicene). In fact, the silver-heptahelicene interaction is stronger than the silver-hexahelicene interaction for the two types of sites (M and P) at the four temperatures. This result indicates that the affinity of the receptor sites of the heptahelicene surface to the silver ions is more important compared to the hexahelicene sites and confirms that the heptahelicene is the best complexing adsorbent of silver.

Moreover, the adsorption energies of hexahelicene are less than 40 kJ/mol indicating physical adsorption process [47–50]. This type of adsorption is weakly energetic, and there is no redistribution of the electron density either of the adsorbed particle or of the adsorbent surface; the adsorbed particles retain their individual properties. Physical adsorption (physisorption) is generally a reversible phenomenon so the interaction adsorbate-adsorbent is weak and the presence of an opposite phenomenon (desorption process) is possible. Indeed, the type of the interaction can be classified, to a certain extent, by the magnitude of the change in adsorption energy [46, 49]. The values of the adsorption energies of hexahelicene can be classified into electrostatic bindings [15, 48].

On the other hand, all the energies of heptahelicene are superior to 80 kJ/mol for all the temperatures. Therefore, we conclude that the complexation of heptahelicene by the cationic silver is a chemical adsorption process involving ionic or covalent bonds [40, 50]. Chemical adsorption process (chemisorption) is generally an irreversible phenomenon and accompanies with the presence of a strong bond between the adsorbate and the adsorbent (the formation of double liaison is possible). During chemisorption, new chemical bonds are formed between the adsorbent surface and the adsorbed particles. In the case of chemisorption, where the adsorbed particles undergo a change in structure and a rearrangement of the electron density between the adsorbed particle and the adsorbent surface, the chemical adsorption is a dissociative process. Therefore, a desorption process is almost impossible due to the strong interaction adsorbate-adsorbent [40].

The variations of the adsorption energies via the temperature are illustrated in Figure 4(c).

It is noted that the adsorption energies (in modulus) $|(-\Delta E_1)|$ and $|(-\Delta E_2)|$ increase with the rise of the temperature. This is explained by the endothermic character of the two adsorption mechanisms [36].

The next section is devoted to the thermodynamic evaluation which leads to better interpret the macroscopic behavior of the adsorption processes.

4. Thermodynamic Study

The statistical physics treatment is used for the development of three potential thermodynamic functions which are the configurational entropy, the Gibbs free enthalpy, and the internal energy [37, 51, 52].

4.1. Configurational Entropy. The importance of this thermodynamic function is to give useful information describing the behavior of the adsorbate ions at the adsorbent surface. In our case, we only focus on the configurational aspect of the entropy which describes the disorder during the adsorption process [53, 54]. Using the grand canonical partition function related to the fitting model, the grand potential J can be written as follows [54]:

$$J = -k_B T \ln z_{gc} = -\frac{\partial \ln z_{gc}}{\partial \beta} - TS_a. \tag{17}$$

The entropy expression S_a/k_B (J·K^{-1}) can be deduced from this equation [46, 54]:

$$\frac{S_a}{k_B} = -\beta \frac{\partial \ln\left(z_{gc}\right)}{\partial \beta} + \ln\left(z_{gc}\right). \tag{18}$$

Then, the configurational entropy has the following expression.

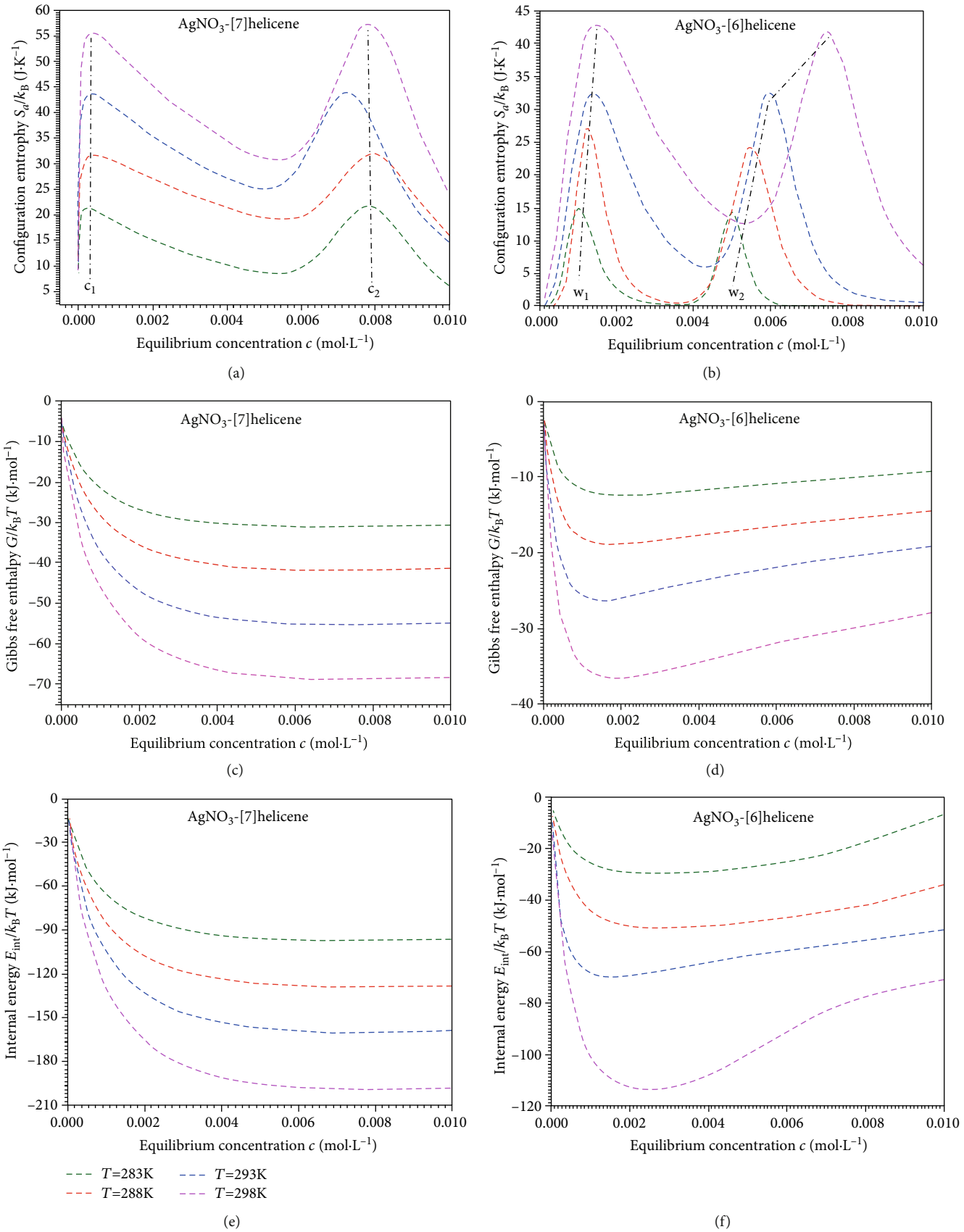

FIGURE 5: Evolutions of (a, b) the configurational entropy S_a/k_B (J·K^{-1}), (c, d) the Gibbs free enthalpy G/k_BT (kJ·mol^{-1}), and (e, f) the internal energy E_{int}/k_BT (kJ·mol^{-1}) as a function of equilibrium concentration and temperature.

For the adsorption system silver nitrate-heptahelicene (SMPG model),

$$\frac{S_a}{k_B} = \left[H_{m1} \ln\left(1 + \left(\frac{c}{c_1}\right)^{n1}\right) + H_{m2} \ln\left(1 + \left(\frac{c}{c_2}\right)^{n2}\right)\right] - \left[\left(\frac{H_{m1}(c/c_1)^{n1} \ln\left((c/c_1)^{n1}\right)}{1 + (c/c_1)^{n1}}\right) + \left(\frac{H_{m2}(c/c_2)^{n2} \ln\left((c/c_2)^{n2}\right)}{1 + (c/c_2)^{n2}}\right)\right]. \quad (19)$$

For the adsorption system silver nitrate-hexahelicene (SMPG model),

$$\frac{S_a}{k_B} = [H_{m1} \ln(1 + x_1) + H_{m2} \ln(1 + x_2)] - \left[\left(\frac{H_{m1}x_1 \ln(x_1)}{1 + x_1}\right) + \left(\frac{H_{m2}x_2 \ln(x_2)}{1 + x_2}\right)\right], \quad (20)$$

where x_1 and x_2 are expressed as follows:

$$x_1 = \left(\frac{c}{w_1(1 - bc)e^{2\beta ac}e^{-bc/(1-bc)}}\right)^{n1}, \quad (21)$$

$$x_2 = \left(\frac{c}{w_2(1 - bc)e^{2\beta ac}e^{-bc/(1-bc)}}\right)^{n2}. \quad (22)$$

Figures 5(a) and 5(b) depict the evolutions of the entropy of the two adsorption systems.

It can be noticed that the entropy does not vary linearly as a function of concentration. One can see that both entropies follow two different behaviors below and above the energetic parameters. At low concentrations, the silver ion has numerous empty sites which lead to various possibilities to choose one to be adsorbed. Therefore, the disorder is important on the adsorbent surface. When the concentration is equal to c_1 or c_1 (Figure 5(a)) and w_1 or w_2 (Figure 5(b)), the disorder reaches its maximum values [46]. After these particular points, the adsorbate ion has low probability to choose an adsorbent site since the helicene surface tends towards order and the two adsorption systems tends towards saturation.

It can be also noted that the two peaks of the two adsorption systems are nearly equal since the energetic parameters (c_1 and c_1 for heptahelicene and w_1 and w_2 for hexahelicene) describe the same type of interaction which is between the silver ions and the two spatial conformations (M and P) of the two helicenes.

About the effect of the temperature, one can note that for a fixed concentration, the higher the temperature the greater the entropy. Indeed, the higher the adsorbed quantities, the greater the disorder.

4.2. Gibbs Free Enthalpy. It is useful to investigate the change in the free enthalpy for the adsorption systems. Thus, any reaction for which the change in the Gibbs free enthalpy is negative should be favorable or spontaneous. This thermodynamic function is calculated using the adsorbed quantity expression of the fitting model as follows [37, 46]:

$$G = \mu * Q_m. \quad (23)$$

For the adsorption system silver nitrate-heptahelicene, we use the chemical potential μ_p given by Equation (7) and the expression of the adsorbed quantity Q_{SMPG} of the SMPG model (Equation (11)) to deduce the free enthalpy expression G/k_BT (kJ·mol^{-1}):

$$\frac{G}{k_BT} = \ln\left(\frac{c}{z_{Tr}}\right) * \left[\frac{(c/c_1)^{n1}Q_{S1}}{1 + (c/c_1)^{n1}} + \frac{(c/c_2)^{n2}Q_{S2}}{1 + (c/c_2)^{n2}}\right]. \quad (24)$$

For the adsorption system silver nitrate-hexahelicene, we use the chemical potential μ_r given by Equation (9) and the expression of the adsorbed quantity Q_{SMRG} of the SMRG model (Equation (13)):

$$\frac{G}{k_BT} = \left[\ln\left(\frac{c}{z_{Tr}}\right) + \ln\frac{1}{1 - bc} + \frac{bc}{1 - bc} - \frac{2ac}{k_BT}\right] * \left[\frac{x_1Q_{S1}}{1 + x_1} + \frac{x_2Q_{S2}}{1 + x_2}\right], \quad (25)$$

where x_1 and x_2 are given by Equations (21) and (22).

The evolutions of the Gibbs free enthalpy of the two adsorption systems are depicted in Figure 5(c) for heptahelicene adsorption and in Figure 5(d) for hexahelicene adsorption.

For the two helicenes, it is noticed that the adsorption reaction evolves spontaneously since the free enthalpy is always negative [45]. At the beginning of the complexation process, the helicene sites are almost empty which leads to strong interaction adsorbate-adsorbent. Then, the enthalpy values decrease with increasing the silver nitrate concentration until it reaches the equilibrium state.

4.3. Internal Energy. The internal energy concept is an indispensable tool for the understanding of the physicochemical phenomena such as the case of adsorption process. Using the statistical physics formalism, the internal energy is given by [46]

$$E_{int} = -\frac{\partial \ln(z_{gc})}{\partial \beta} + \frac{\mu}{\beta}\left(\frac{\partial \ln(z_{gc})}{\partial \mu}\right). \quad (26)$$

For the adsorption system silver nitrate-heptahelicene (SMPG model), it can be written in the following expression:

$$\frac{E_{\text{int}}}{k_B T} = \ln\left(\frac{c}{z_{\text{Tr}}}\right) * \left[\left(\frac{(c/c_1)^{n1} H_{m1}}{1+(c/c_1)^{n1}}\right) + \left(\frac{(c/c_2)^{n2} H_{m2}}{1+(c/c_2)^{n2}}\right)\right] - \left[\left(\frac{H_{m1}(c/c_1)^{n1} \ln\left((c/c_1)^{n1}\right)}{1+(c/c_1)^{n1}}\right) + \left(\frac{H_{m2}(c/c_2)^{n2} \ln\left((c/c_2)^{n2}\right)}{1+(c/c_2)^{n2}}\right)\right]. \tag{27}$$

For the adsorption system silver nitrate-hexahelicene (SMRG model), it has the following formula:

$$\frac{E_{\text{int}}}{k_B T} = \left[\ln\left(\frac{c}{z_{\text{Tr}}}\right) + \ln\frac{1}{1-bc} + \frac{bc}{1-bc} - \frac{2ac}{k_B T}\right] * \left[\left(\frac{x_1 H_{m1}}{1+x_1}\right) + \left(\frac{x_2 H_{m2}}{1+x_2}\right)\right] - \left[\left(\frac{H_{m1} x_1 \ln(x_1)}{1+x_1}\right) + \left(\frac{H_{m2} x_2 \ln(x_2)}{1+x_2}\right)\right], \tag{28}$$

with x_1 and x_2 previously mentioned (Equations (21) and (22)).

We depicted the evolutions of the internal energy in Figure 5(e) (heptahelicene adsorption) and Figure 5(f) (hexahelicene adsorption).

It can be noticed that the internal energy is negative for the two helicenes. The two adsorption systems tend to decrease their internal energy, and the two complexation processes evolve spontaneously until the saturation state [46]. Interestingly, it can be observed that the complexation mechanism of heptahelicene evolves towards a stable saturation level (Figure 5(e)). On the contrary, the internal energy of hexahelicene (Figure 5(f)) is not constant at high concentrations, but it increases in algebraic value (decreases in modulus). Indeed, the silver-hexahelicene interaction is important at the beginning of the adsorption process. Then, this value decreases; it is possibly due to the adsorbate-adsorbate interaction (lateral interactions) which becomes strong at high concentration to prevent the adsorption process [37].

5. Conclusion

The adsorption of silver onto helicene molecules is studied by the grand canonical ensemble in statistical physics, to find new microscopic interpretations. The adsorption measurements are successfully carried out using a quartz crystal microbalance. Through the experimental result discussion, it is discovered that the heptahelicene is the best complexing adsorbent of silver because it shows the highest adsorption capacities. Two single-layer adsorption models with two energy levels (SMPG and SMRG) are developed and applied for these systems. It is found that the proposed statistical treatment is sufficiently flexible to give a good representation of the experimental data. Some physicochemical parameters related to the adsorption processes are introduced in the analytical model expressions, and they are directly obtained from the fitting of the experimental adsorption isotherms by numerical simulation. This is in the aim to explain the behavior of silver ion versus helicene molecules. The evolutions of the adsorbed quantities at saturation versus temperature demonstrate the endothermicity of the adsorption process of the two members of the helicene family. The energetic interpretation shows that the silver ions are physisorbed onto hexahelicene, whereas chemical bonds are explored between the [7]helicene and the silver.

The SMPG model and the SMRG model are also applied to calculate three thermodynamic functions which govern the adsorption mechanisms. Through the entropy behavior, we notice that the disorder reaches two maximums when the adsorbate concentration is equal to the energetic parameters where the adsorption process reactivity is at its maximum. It is also noted that the Gibbs free enthalpy and the internal energy are negative which proved that during the complexation process the two adsorption systems evolve spontaneously towards the saturation level. It is also found that the lateral interactions between the adsorbates act intensively at high concentration to forestall the hexahelicene adsorption.

Data Availability

The data that supports the findings of this study are available within the article.

Conflicts of Interest

There are no known conflicts of interest associated with this publication.

References

[1] N. Saleh, C. Shen, and J. Crassous, "Helicene-based transition metal complexes: synthesis, properties and applications," *Chemical Science*, vol. 5, no. 10, pp. 3680–3694, 2014.

[2] H. Tanaka, M. Ikenosako, Y. Kato, M. Fujiki, Y. Inoue, and T. Mori, "Symmetry-based rational design for boosting chiroptical responses," *Communications Chemistry*, vol. 1, no. 1, pp. 386–402, 2018.

[3] Y. Nakai, T. Mori, and Y. Inoue, "Theoretical and experimental studies on circular dichroism of carbo[n]helicenes," *The Journal of Physical Chemistry A.*, vol. 116, no. 27, pp. 7372–7385, 2012.

[4] K. Nakano, H. Oyama, Y. Nishimura, S. Nakasako, and K. Nozaki, "λ^5-Phospha[7]helicenes: synthesis, properties, and columnar aggregation with one-way chirality†," *Angewandte Chemie International Edition*, vol. 51, no. 3, pp. 695–699, 2012.

[5] J. Žádný, P. Velíšek, M. Jakubec, J. Sýkora, V. Církva, and J. Storch, "Exploration of 9-bromo[7]helicene reactivity," *Tetrahedron*, vol. 69, no. 30, pp. 6213–6218, 2013.

[6] D. Mendola, N. Saleh, N. Hellou et al., "Synthesis and structural properties of aza[n]helicene platinum complexes: control of cis and trans stereochemistry," *Inorganic Chemistry*, vol. 55, no. 5, pp. 2009–2017, 2016.

[7] M. Šámal, S. Chercheja, J. Rybáček et al., "An ultimate stereocontrol in asymmetric synthesis of optically pure fully

aromatic helicenes," *Journal of the Americal Chemical Society*, vol. 137, no. 26, pp. 8469–8474, 2015.

[8] N. Takenaka, J. Chen, B. Captain, R. S. Sarangthem, and A. Chandrakumar, "Helical chiral 2-aminopyridinium ions: a new class of hydrogen bond donor catalysts," *Journal of the Americal Chemical Society*, vol. 132, no. 13, pp. 4536-4537, 2010.

[9] D. Dova, S. Cauteruccio, S. Prager, A. Dreuw, C. Graiff, and E. Licandro, "Chiral thiahelicene-based alkyl phosphine–borane complexes: synthesis, X-ray characterization, and theoretical and experimental investigations of optical properties," *The Journal of Organic Chemistry*, vol. 80, no. 8, pp. 3921–3928, 2015.

[10] F. Dumitrascu, D. G. Dumitrescu, and I. Aron, "Azahelicenes and other similar tri and tetracyclic helical molecules," *ARKIVOC*, vol. 1, pp. 1–32, 2010.

[11] J. OuYang and J. Crassous, "Chiral multifunctional molecules based on organometallic helicenes: recent advances," *Coordination Chemistry Reviews*, vol. 376, pp. 533–547, 2018.

[12] J. Chen, B. Captain, and N. Takenaka, "Helical chiral 2,2′ -bipyridineN-monoxides as catalysts in the enantioselective propargylation of aldehydes with allenyltrichlorosilane," *Organic Letters*, vol. 13, no. 7, pp. 1654–1657, 2011.

[13] M. J. Fuchter, J. Schaefer, D. K. Judge, B. Wardzinski, M. Weimar, and I. Krossing, "[7]-Helicene: a chiral molecular tweezer for silver(I) salts," *Dalton Transactions*, vol. 41, no. 27, pp. 8238–8241, 2012.

[14] D. Vijay and G. N. Sastry, "Exploring the size dependence of cyclic and acyclic π-systems on cation–π binding†," *Physical Chemistry Chemical Physics*, vol. 10, no. 4, pp. 582–590, 2008.

[15] M. B. Yahia, S. Knani, L. B. H. Hsan, M. B. Yahia, H. Nasri, and A. B. Lamine, "Statistical studies of adsorption isotherms of iron nitrate and iron chloride on a thin layer of porphyrin," *Journal of Molecular Liquids*, vol. 248, pp. 235–245, 2017.

[16] M. B. Yahia, F. Aouaini, M. B. Yahia, E. S. Almogait, and H. al-Ghamdi, "Theoretical investigation of the chlorophyll nucleus adsorption monitored with quartz crystal microbalance technique: new insights on physicochemical properties," *Journal of Molecular Liquids*, vol. 289, pp. 111188-111189, 2019.

[17] B. Klepetářová, E. Makrlík, D. Sýkora, S. Böhm, and P. Vaňura, "Cation-π interaction of the univalent silver cation with racemic [6]helicene in the gas phase and in the solid state," *Polyhedron*, vol. 117, pp. 1–6, 2016.

[18] B. Klepetářová, E. Makrlík, J. J. Dytrtová, S. Böhm, P. Vaňura, and J. Storch, "[6]Helicene as a novel molecular tweezer for the univalent silver cation: experimental and theoretical study," *Journal of Molecular Structure*, vol. 1097, pp. 124–128, 2015.

[19] E. Makrlík, J. Jaklová Dytrtová, P. Vaňura, J. Sýkora, Vladimír Církva, and J. Storch, "Cation-π interaction of Ag^+ with [6]helicene: An experimental and theoretical study," *Chemical Physics Letters*, vol. 633, pp. 105–108, 2015.

[20] F. Riobé, R. Szűcs, C. Lescop et al., "Coordination complexes of P-containing polycyclic aromatic hydrocarbons: optical properties and solid-state supramolecular assembly," *Organometallics*, vol. 36, no. 14, pp. 2502–2511, 2017.

[21] M. P. Johansson and M. Patzschke, "Fixing the chirality and trapping the transition state of helicene with atomic metal glue," *Chemistry: A European Journal*, vol. 15, no. 47, pp. 13210–13218, 2009.

[22] S. Knani, N. Khalifa, M. Ben Yahia, F. Aouaini, and M. Tounsi, "Statistical physics study of the interaction of the 5, 10, 15, 20-tetrakis (4-tolylphenyl) porphyrin (H_2TTPP) with magnesium ion: new microscopic interpretations," *Arabian Journal of Chemistry*, vol. 13, no. 2, pp. 4374–4385, 2020.

[23] J. H. Lee, H. R. Kim, J. H. Lee et al., "Enhanced in-vitro hemozoin polymerization by optimized process using histidine-rich protein II (HRPII)," *Polymers*, vol. 11, no. 7, pp. 1162–1162, 2019.

[24] G. Sener, E. Ozgur, E. Yılmaz, L. Uzun, R. Say, and A. Denizli, "Quartz crystal microbalance based nanosensor for lysozyme detection with lysozyme imprinted nanoparticles," *Biosensensors and Bioelectronics*, vol. 26, no. 2, pp. 815–821, 2010.

[25] S. Korposh, R. Selyanchyn, and S. W. Lee, "Nano-assembled thin film gas sensors. IV. Mass-sensitive monitoring of humidity using quartz crystal microbalance (QCM) electrodes," *Sensors and Actuators B: Chemical*, vol. 147, no. 2, pp. 599–606, 2010.

[26] J. C. Yang, J. Lee, S. W. Hong, and J. Park, "Molecularly imprinted quartz crystal microbalance sensors with lithographically patterned frisbee-like pillar arrays for sensitive and selective detection of iprodione," *Sensors and Actuators B: Chemical*, vol. 320, pp. 128366-128367, 2020.

[27] U. Latif, S. Can, H. F. Sussitz, and F. L. Dickert, "Molecular imprinted based quartz crystal microbalance sensors for bacteria and spores†," *Chemosensors*, vol. 8, no. 3, pp. 64-65, 2020.

[28] S. Knani, N. Mabrouk, M. Tounsi, and M. Ben Yahia, "Statistical modeling of adsorption isotherm of potassium on aza[7]-helicene-coated gold electrode attached to quartz crystal microbalance," *Separation Science and Technology*, vol. 54, no. 15, pp. 2386–2396, 2019.

[29] S. Kravchenko and B. Snopok, ""Vanishing mass" in the Sauerbrey world: quartz crystal microbalance study of self-assembled monolayers based on a tripod-branched structure with tuneable molecular flexibility†," *Analyst*, vol. 145, no. 2, pp. 656–666, 2020.

[30] C. S. Hodges, D. Harbottle, and S. Biggs, "Investigating adsorbing viscoelastic fluids using the quartz crystal microbalance," *ACS Omega*, vol. 5, no. 35, pp. 22081–22090, 2020.

[31] P. Buck, E. Lindner, W. Kutner, and G. Inzelt, "Piezoelectric chemical sensors (IUPAC technical report)," *Pure and Applied Chemistry*, vol. 76, no. 6, pp. 1139–1160, 2004.

[32] K. A. Marx, "Quartz crystal microbalance: a useful tool for studying thin polymer films and complex biomolecular systems at the solution-surface interface," *Biomacromolecules*, vol. 4, no. 5, pp. 1099–1120, 2003.

[33] W. Shan, Y. Pan, H. Fang et al., "An aptamer-based quartz crystal microbalance biosensor for sensitive and selective detection of leukemia cells using silver-enhanced gold nanoparticle label," *Talanta*, vol. 126, pp. 130–135, 2014.

[34] J. F. Art, P. Soumillion, and C. C. Dupont-Gillain, "Use of a quartz crystal microbalance platform to study protein adsorption on aluminum hydroxide vaccine adjuvants: focus on phosphate-hydroxide ligand exchanges," *International Journal of Pharmaceutics*, vol. 573, pp. 118834-118835, 2020.

[35] L. M. Pandey, "Surface engineering of personal protective equipments (PPEs) to prevent the contagious infections of SARS-CoV-2," *Surface Engineering*, vol. 36, no. 9, pp. 901–907, 2020.

[36] A. Nakbi, M. Bouzid, F. Ayachi, F. Aouaini, and A. Ben Lamine, "Investigation of caffeine taste mechanism through a statistical physics modeling of caffeine dose-taste response curve by a biological putative caffeine adsorption process in

electrophysiological response," *Progress in Biophysics and Molecular Biology*, vol. 149, pp. 70–85, 2019.

[37] M. B. Yahia, M. B. Yahia, F. Aouaini et al., "Adsorption of sodium and lithium ions onto helicenes molecules: Experiments and phenomenological modeling," *Journal of Molecular Liquids*, vol. 288, p. 110998, 2019.

[38] R. Ezzati, "Derivation of pseudo-first-order, pseudo-second-order and modified pseudo-first-order rate equations from Langmuir and Freundlich isotherms for adsorption," *Chemical Engineering Journal*, vol. 392, pp. 123705-123706, 2020.

[39] J. A. V. Rodrigues, L. R. Martins, L. M. Furtado et al., "Oxidized renewable materials for the removal of cobalt(II) and copper(II) from aqueous solution using in batch and fixed-bed column adsorption," *Effects of anesthetic agents on the fetus and newborn*, vol. 2020, article 8620431, pp. 1–17, 2020.

[40] J. Barroso, J. L. Cabellos, S. Pan et al., "Revisiting the racemization mechanism of helicenes†," *Chemical Communications*, vol. 54, no. 2, pp. 188–191, 2018.

[41] S. Wjihi, F. Aouaini, A. Erto, M. Balsamo, and A. B. Lamine, "Advanced interpretation of CO_2 adsorption thermodynamics onto porous solids by statistical physics formalism," *Chemical Engineering Journal*, vol. 406, pp. 126669-126670, 2021.

[42] L. D. T. Prola, E. Acayanka, E. C. Lima et al., "Comparison of *Jatropha curcas* shells in natural form and treated by non-thermal plasma as biosorbents for removal of reactive red 120 textile dye from aqueous solution," *Industrial Crops and Products*, vol. 46, pp. 328–340, 2013.

[43] M. Hadi, M. R. Samarghandi, and G. McKay, "Equilibrium two-parameter isotherms of acid dyes sorption by activated carbons: study of residual errors," *Chemical Engineering Journal*, vol. 160, no. 2, pp. 408–416, 2010.

[44] T. V. Rêgo, T. R. S. Cadaval, G. L. Dotto, and L. A. A. Pinto, "Statistical optimization, interaction analysis and desorption studies for the azo dyes adsorption onto chitosan films," *Journal of Colloid and Interface Science*, vol. 411, pp. 27–33, 2013.

[45] M. Ben Yahia, M. Tounsi, F. Aouaini, S. Knani, M. Ben Yahia, and A. Ben Lamine, "A statistical physics study of the interaction of [7]-helicene with alkali cations (K^+ and Cs^+): new insights on microscopic adsorption behavior," *RSC. Advances*, vol. 7, no. 71, pp. 44712–44723, 2017.

[46] H. Alyousef, M. Ben Yahia, and F. Aouaini, "Statistical physics modeling of water vapor adsorption isotherm into kernels of dates: experiments, microscopic interpretation and thermodynamic functions evaluation," *Arabian Journal of Chemistry*, vol. 13, no. 3, pp. 4691–4702, 2020.

[47] B. Mohamed, Z. Qingyu, G. D. Moggridge, and B. L. Abdelmottaleb, "New insight in adsorption of pyridine on the two modified adsorbents types MN200 and MN500 by means of grand canonical ensemble," *Journal of Molecular Liquids*, vol. 263, pp. 413–421, 2018.

[48] S. Saini and B. M. Deb, "A computational study of the interaction of [7]-helicene with alkali cations and benzene," *Indian Journal of Chemistry A*, vol. 46, pp. 9–15, 2007.

[49] C. L. Sun and C. S. Wang, "Estimation on the intramolecular hydrogen-bonding energies in proteins and peptides by the analytic potential energy function," *Journal of Molecular Structure*, vol. 956, no. 1-3, pp. 38–43, 2010.

[50] H. Zheng, Z. Wang, J. Zhao, S. Herbert, and B. Xing, "Sorption of antibiotic sulfamethoxazole varies with biochars produced at different temperatures," *Environmental Pollution*, vol. 181, pp. 60–67, 2013.

[51] P. Senthil Kumar, S. Ramalingam, C. Senthamarai, M. Niranjanaa, P. Vijayalakshmi, and S. Sivanesan, "Adsorption of dye from aqueous solution by cashew nut shell: studies on equilibrium isotherm, kinetics and thermodynamics of interactions," *Desalination*, vol. 261, no. 1-2, pp. 52–60, 2010.

[52] M. D. Liébanes, J. M. Aragón, M. C. Palancar, G. Arévalo, and D. Jiménez, "Equilibrium moisture isotherms of two-phase solid olive oil by-products: adsorption process thermodynamics," *Colloids and Surfaces A: Physicochemical and Engineering Aspects*, vol. 282-283, pp. 298–306, 2006.

[53] O. Hamdaoui and E. Naffrechoux, "Modeling of adsorption isotherms of phenol and chlorophenols onto granular activated carbon: Part I. Two-parameter models and equations allowing determination of thermodynamic parameters," *Journal of Hazardous Materials*, vol. 147, no. 1-2, pp. 381–394, 2007.

[54] M. Ben Yahia and M. Ben Yahia, "New insights in the physicochemical investigation of the vitamin B12nucleus using statistical physics treatment: interpretation of experiments and surface properties," *RSC. Advances*, vol. 10, no. 37, pp. 21724–21735, 2020.